Modeling Methods for the Design of 3D Broadcloth Composite Parts

Masaki Aono[†], David E. Breen[*], and Michael J. Wozny[‡]

[†]Tokyo Research Laboratory, IBM Japan Ltd., Kanagawa, Japan
[*]Computer Graphics Lab, California Institute of Technology, Pasadena, CA
[‡]Center for Automation Technologies, Rensselaer Polytechnic Institute, Troy, NY

1 Introduction

With the advent of lighter and stronger composite materials over the last two decades, more and more metals have been replaced by composite materials in aircraft and other vehicles. It is not suprising that the airframes of certain aircraft (e.g. Lear Fan 2100) are totally fabricated from composite materials. Composites consist of a reinforcing material suspended in a "matrix" material (e.g. epoxy) that bonds it to adjacent reinforcing materials. The three major composite forms are chopped fiber, unidirectional tape, and (bidirectional) broadcloth.

Today's aircraft mostly employ broadcloth composites partly because they have outstanding strength-to-weight ratio, and partly because their structural properties may be tailored to the expected load in different directions [16]. Broadcloth composites have both vertical and horizontal threads (weft and warp) interwoven to form a sheet of cloth as seen in Fig 1. They strongly resist stretching along thread directions, but can be deformed flexibly along thread diagonals by changing the angle between vertical and horizontal threads. This allows a composite broadcloth to be "formed" into virtually any curved surface. In order to reinforce aircraft structures, multiple sheets (plies) of broadcloth composites are usually laid one on top of the other, a lamination process.

With this trend of replacing metals with composite materials, new lamination technologies have been developed to manufacture composite materials in order to form an airframe. During the lamination process, plies of composite sheets must be cut to the required size, with the required fiber orientation, and laid up onto the surface of a die or molding tool prior to curing. It is this process of deforming a broadcloth composite sheet into a 3D shape by pressing it onto a mold that we will refer to as a "fitting." Unfortunately, the cutting and orientation process has not yet been fully automated, and it has been mostly implemented with manual procedures. It is therefore a time-consuming, non-reproducable, and inaccurate process in need of design automation tools.

In this paper we present a number of modeling methods that may be used to automate the design of 3D broadcloth composite parts. First, we describe a model (a Tchebychev net) which allows us to simulate the deformation of woven materials into a specific 3D shape. Two algorithms are described for performing the actual fitting. The first algorithm simulates the fit by solving the Tchebychev net formula using a finite difference technique. The second algorithm simulates the fit by reducing the problem to a surface-surface intersection problem.

Once we establish the techniques for simulating a fit, we can discuss the quality and acceptibility of the fit. In general, a good fit is the one that consumes the smallest area of the material, that has the smallest deformation energy, and that is free of manufacturing anomalies such as wrinkles and breaks. We will present mathematical tools that allow us to measure the "goodness" of a fit with a Tchebychev net, and that allow us to visually identify where a possible anomalous event may occur. Specifically, we will introduce a path-dependent Gaussian curvature integral that is defined at an arbitrary point in a surface region. With a path-dependent Gaussian curvature integral, we will show that it is possible not only to predict anomalous events, or wrinkles in particular, but to provide a solution to preventing them. Finally, we will propose three methods for preventing anomalous events: (1) automatic generation of a good initial condition, (2) dart insertion, and (3) surface shape modification. Providing different methods for preventing

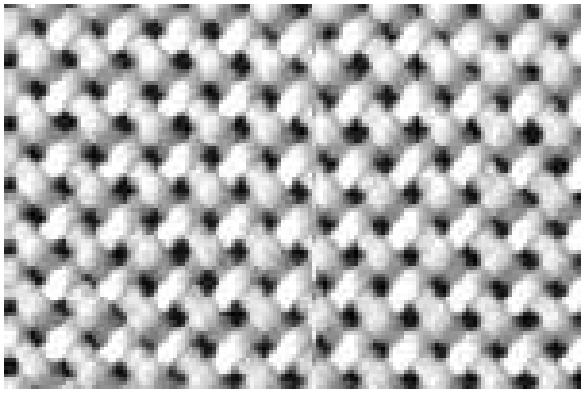

Figure 1: A close-up of woven cloth fiberglass sheet.

anomalous events allows a designer of broadcloth composites to select any combination of them in accordance with his/her design task. The ultimate goal of all of these techniques is to provide a designer the software tools needed to easily determine the shape of the broadcloth plies needed to cover a specific 3D shape.

2 Previous Work

Research on the "fit" of a sheet of woven cloth fabrics was initiated by Mack and Taylor [17] and has been investigated chiefly in the textile and polymer industry. Mack and Taylor's model was similar to a Tchebychev net in that the threads are assumed to be inextensible. However, their model could only be used on a surface of revolution. Heisey and Haller [15] first attempted to numerically solve a differential equation similar to Mack and Taylor's. Robertson et al. [25] and Van West et al. [35] considered the fit of a sheet of woven cloth composites and reduced the problem to an intersection calculation between two spheres and the surface that is modeled by either a quadric or a Hermite patch. Unfortunately, these previous approaches either cannot be applied to a general free-form surface or lack flexibility in specifying a variety of initial conditions. To our knowledge, no previous methods that prevent anomalous events have been proposed. Prakash et al. [23] describe an interactive system for designing aircraft composite components. They model a ply as a set of polygons and their composite forms are assumed to be unidirectional tapes. Therefore, their method for approximating flat pattern development can only be applied to a limited set of 3D surface shapes such as strips, panel and shell type components which have shallow curvatures. Recently McCartney et al. [19] and Fan et al. [11] have presented techniques for flattening 3-D cloth surfaces into 2-D flat patterns. We do not believe that this is the correct approach to generating patterns for 3-D cloth structures. We will show that a 3-D structure can be produced by significantly different 2-D patterns, depending on the process that deforms the cloth. It is only through the forward simulation of the deformation process can one be confident that the correct 2-D pattern is produced.

Our work provides several significant advances over previous work. These advances are:

- flexibility in representing and controlling the modelled 3D surface with NURBS surfaces,
- the ability to simulate a great variety of fittings, based on a flexible method for specifying initial conditions,
- the ability to confidently predict the 2D flattened pattern necessary for producing a composite ply fitted to a given 3D surface region,
- the ability to automatically insert darts where excessive shear deformation is predicted,
- the ability to automatically provide good initial conditions that lead to the smallest possibility of anomalous events such as wrinkling and tearing, given a fixed 3D surface shape,
- the ability to modify the surface into a shape that is less likely to produce anomalous events, given fixed initial conditions,
- the ability to produce a variety of visualizations for evaluating a fitting result.

3 A Tchebychev Net Cloth Model

Within computer graphics cloth models [20] are identified as either physically-based [1, 7, 33], geometry-based [37], or a combination of both [8, 27]. We present a geometry-based cloth model called a Tchebychev net in which cloth is assumed to be made of inextensible threads. Ever since Tchebychev proposed a model of cloth in his lecture in the late 19th century [32], Tchebychev nets have been investigated mainly in the fields of differential geometry [9, 28, 29, 30] and mechanical engineering [21, 24, 36]. We have explored a new application of Tchebychev nets in the simulation of the "fit" of a sheet of woven cloth composites [2, 3, 4].

Woven cloth composites have a Young's modulus in the thread direction that is usually ten to hundred times larger than its shear modulus [10]. This is in sharp contrast to conventional fabrics such as wool and cotton in which the Young's modulus is much smaller and is closer to the shear modulus. Because of this property we can regard a sheet of woven cloth composites as a Tchebychev net. In other words, deformation of the composite cloth is produced by changing the angle between vertical and horizontal threads, and the extension of its threads can be neglected without much loss of accuracy. This salient feature allows us to efficiently simulate the fit of a sheet of woven cloth composites with only geometric information.

3.1 A Fundamental Equation of a Tchebychev Net

A Tchebychev net is a continuum model for cloth in which the threads are treated as continuously distributed and inextensible. Without loss of generality, we assume that a deformed 3D Tchebychev net from an initially flat 2D net forms a differentiable manifold. Suppose (x, y) represents an intersection between a vertical thread called *warp* and a horizontal thread called *weft* in a 2D sheet of woven cloth composites. Consider a location $(x + dx, y)$ along a weft, and a location $(x, y + dy)$ along a warp, where dx and dy are sufficiently small positive values. We then consider mapping three points ((x, y), $(x + dx, y)$, and $(x, y + dy)$) onto a 3D surface. Suppose that (x, y) is mapped to (u, v), the coordinate of the point represented in a bivariate parametric space. Suppose also that the surface is C^∞ differentiable everywhere. Then, by applying Taylor's theorem to the first order partials around the point (u, v), the point $(x+dx, y)$ is mapped to $(u+\frac{\partial u}{\partial x}dx, v+\frac{\partial v}{\partial x}dx)$, and the point $(x, y+dy)$ is mapped to $(u+\frac{\partial u}{\partial y}dy, v+\frac{\partial v}{\partial y}dy)$ as shown in Figure 2. From the inextensibility assumption, the distance between (u, v) and $(u + \frac{\partial u}{\partial x}dx, v + \frac{\partial v}{\partial x}dx)$ must be equal to dx, and the distance between (u, v) and $(u + \frac{\partial u}{\partial y}dy, v + \frac{\partial v}{\partial y}dy)$ must be equal to dy. We therefore obtain the following pair of equations:

$$\left.\begin{array}{l} \left(\frac{\partial u}{\partial x}\right)^2 + \left(\frac{\partial v}{\partial x}\right)^2 = 1 \\ \left(\frac{\partial u}{\partial y}\right)^2 + \left(\frac{\partial v}{\partial y}\right)^2 = 1 \end{array}\right\}. \tag{1}$$

Equation (1) can be concisely put into the following form:

$$\left.\begin{array}{l} |\mathbf{r}_x| = 1 \\ |\mathbf{r}_y| = 1 \end{array}\right\}, \tag{2}$$

where $\mathbf{r}_x = (\frac{\partial u}{\partial x}, \frac{\partial v}{\partial x})$ and $\mathbf{r}_y = (\frac{\partial u}{\partial y}, \frac{\partial v}{\partial y})$.

Equation (1) (or equivalently Equation (2)) represents a fundamental equation for a Tchebychev net composed of continuous inextensible threads. It is a system of non-linear hyperbolic partial differential equations. Similarly we can obtain the first fundamental form [30, 31] for a 3D Tchebychev net. Here the arc length element ds is represented by dx and dy in the Tchebychev net coordinate as follows:

$$\begin{aligned} I &= ds^2 \equiv E dx^2 + 2F dxdy + G dy^2 \\ &= |\mathbf{r}_x|^2 dx^2 + 2(\mathbf{r}_x \cdot \mathbf{r}_y) dxdy + |\mathbf{r}_y|^2 dy^2 \\ &= dx^2 + 2\cos\gamma\, dxdy + dy^2, \end{aligned} \tag{3}$$

where γ, the *thread angle*, represents the angle between a weft and a warp. From the above equation, we have $E = G = 1$ and $F = \cos\gamma$, which is another necessary condition for a cloth surface to be a Tchebychev net.

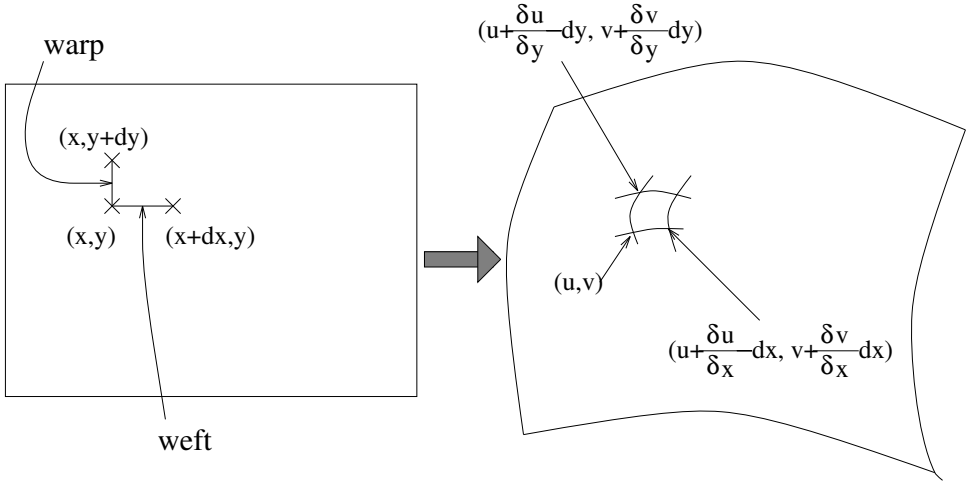

Figure 2: Mapping of a Tchebychev net onto a 3D surface.

3.2 A Numerical Fitting Algorithm for a Tchebychev Net

Here we describe a numerical fitting algorithm for solving Equation (2). From the chain rule we begin with

$$\left.\begin{array}{rcl} \mathbf{r}_x &=& \mathbf{r}_u u_x + \mathbf{r}_v v_x \\ \mathbf{r}_y &=& \mathbf{r}_u u_y + \mathbf{r}_v v_y \end{array}\right\}. \tag{4}$$

By substituting variables $\mathbf{r}_x$ and $\mathbf{r}_y$ in Equation (4) into Equation (3), and by considering $d\mathbf{r} = \mathbf{r}_x dx$ with length $ds = |\mathbf{r}_x|dx = dx$ and $d\mathbf{r} = \mathbf{r}_y dy$ with length $ds = |\mathbf{r}_y|dy = dy$, we obtain the non-linear partial differential equations:

$$\left.\begin{array}{l} Eu_x^2 + 2Fu_x v_x + Gv_x^2 = 1 \\ Eu_y^2 + 2Fu_y v_y + Gv_y^2 = 1 \end{array}\right\}. \tag{5}$$

By differentiating the first equation in (5) with respect to y, and the second equation in (5) with respect to x, we obtain the following system of quasi-linear partial differential equations:

$$\left.\begin{array}{l} u_{xy} = -(u_x u_y \Gamma_{11}^1 + (u_x v_y + u_y v_x)\Gamma_{12}^1 + v_x v_y \Gamma_{22}^1) \\ v_{xy} = -(u_x u_y \Gamma_{11}^2 + (u_x v_y + u_y v_x)\Gamma_{12}^2 + v_x v_y \Gamma_{22}^2) \end{array}\right\}, \tag{6}$$

where Γ_{jk}^i $(i, j, k = 1, 2)$ are the Christoffel's symbols of the second kind [31]. Let $u_{x,y}$ and $v_{x,y}$ denote $u(x, y)$ and $v(x, y)$, respectively. By applying a finite difference method to Equation (6), the point $(u_{x+1,y+1}, v_{x+1,y+1})$ can be expressed by the adjacent points as follows (only for $u_{x+1,y+1}$):

$$\begin{array}{rcl} u_{x+1,y+1} &=& u_{x+1,y-1} + u_{x-1,y+1} - u_{x-1,y-1} \\ &+& A + B + C + D, \end{array} \tag{7}$$

where A, B, C, and D are

$$\begin{array}{rcl} A &=& \Gamma_{11}^1 (u_{x+1,y} - u_{x-1,y})(u_{x,y+1} - u_{x,y-1}), \\ B &=& \Gamma_{12}^1 (u_{x+1,y} - u_{x-1,y})(v_{x,y+1} - v_{x,y-1}), \\ C &=& \Gamma_{12}^1 (v_{x+1,y} - v_{x-1,y})(u_{x,y+1} - u_{x,y-1}), \\ D &=& \Gamma_{22}^1 (v_{x+1,y} - v_{x-1,y})(v_{x,y+1} - v_{x,y-1}). \end{array} \tag{8}$$

In order to solve Equation (7) in the range of $x > 0$ and $y > 0$, we can use the boundary curves such as $u = u(x, 0)$, $u = u(0, y)$, $v = v(x, 0)$, $v = v(0, y)$, $u = u(x, 1)$, $u = u(1, y)$, $v = v(x, 1)$, and $v = v(1, y)$ for the initial conditions. We will refer to such curves as *guide lines* hereafter.

3.3 Intrinsic Geometry and Thread Angle

The first fundamental form of a Tchebychev net given in Equation (3) allows us to derive an interesting relationship between the Gaussian curvature, K, (an intrinsic surface geometric property) and the thread angle, γ.

Lemma 1 *For a 3D surface where a Tchebychev net is fitted, there exists a relationship between the Gaussian curvature K of the surface and the thread angle γ between a weft and a warp, given as follows:*

$$K = -\frac{\gamma_{xy}}{\sin\gamma}, \tag{9}$$

where $\gamma_{xy} = \frac{\partial^2\gamma}{\partial x \partial y}$.

The next lemma states a relationship between the thread angle and the initial thread path. Refer to [3] for the proof.

Lemma 2 *A thread of a Tchebychev net lies along a geodesic path, a curve of zero geodesic curvature, if and only if the thread angle between a weft and a warp is constant along the path.*

An interesting result derived from Lemma 1 relates to the *global conformability* of a sheet of woven cloth composites modeled with a Tchebychev net assumption. By global conformability, we mean that a surface can be fitted with a single sheet of woven cloth composites, assuming that the size of the sheet is sufficiently large. We will also use the term *a global Tchebychev net* for a surface region, if the region has global conformability.

Theorem 1 (Hazzidakis 1880) *There exists no global Tchebychev net for a surface region S, if*

$$|\int\int_S K\, dS| > 2\pi. \tag{10}$$

The theorem states that when the magnitude of the integral Gaussian curvature becomes greater than 2π it is impossible to fit a given surface with a single sheet of woven cloth composites modeled by a Tchebychev net, no matter what initial conditions are specified [14]. The next theorem assures the global conformability when we have a surface whose integral Gaussian curvature is less than $\frac{\pi}{2}$.

Theorem 2 (Samelson 1989) *There exists a global Tchebychev net for a surface region S, if*

$$|\int\int_S K\, dS| < \frac{\pi}{2}. \tag{11}$$

Striclty speaking, this theorem is applied to a surface which is a C^∞-complete, open, simply-connected, two-dimensional Riemannian manifold with compactly supported Gaussian curvature. Samelson proved this theorem by showing the existence of a unique Tchebychev with threads that make angles $\pi/4$ and $3\pi/4$ to a geodesic [28, 29].

Example: A simple example is an entire sphere with radius R. Since the Gaussian curvature of a sphere with radius R is given by: $K \equiv 1/R^2$. Thus,

$$\int\int_S K\, dS = K \int\int_S dS = K \times 4\pi R^2 = 4\pi > 2\pi. \tag{12}$$

It follows that we cannot globally fit a single sheet to an entire sphere, regardless of the materials used. It should be noted that the same is true for any surface homeomorphic to a sphere due to the Gauss-Bonnet theorem [30, 31].

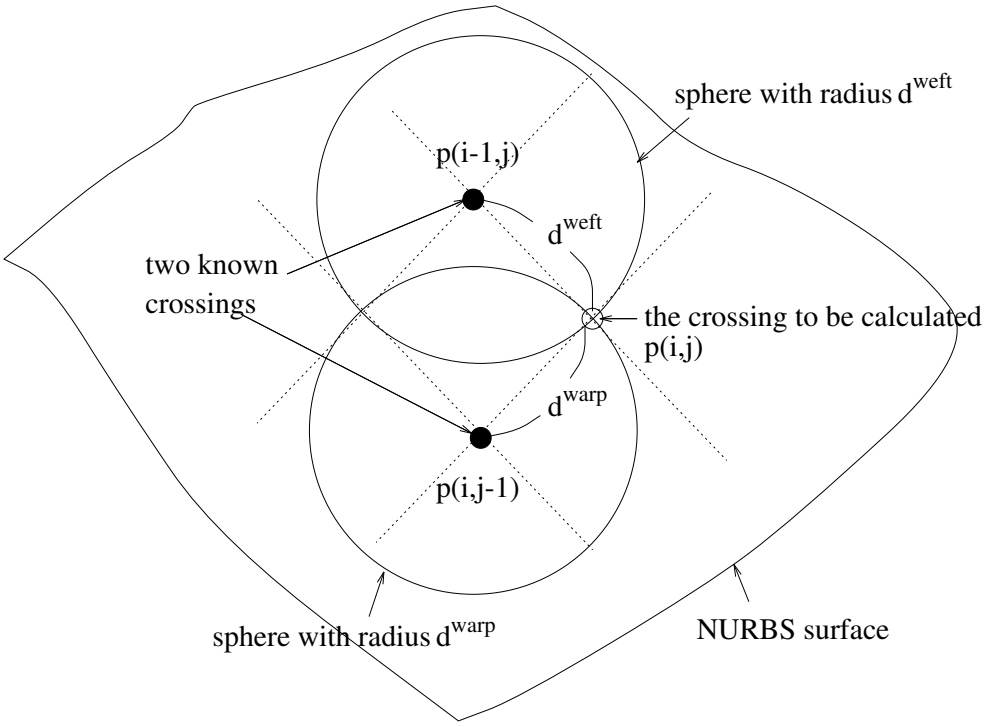

Figure 3: Fitting calculation as a surface-surface intersection problem

4 Simplification of a Fit Problem

Although the numerical fitting algorithm described in Section 3.2 provides a straightforward way to simulate a fit, it is computationally expensive since the second partial derivatives of a given curved surface must be calculated. In addition, it is cumbersome to specify all the necessary initial conditions. In order to simplify a fitting problem, we will introduce additional assumptions. First, we assume that the cloth is modeled by a set of discrete mesh points or *crossings* rather than a continuum. Second, the thread segment between adjacent crossings is assumed to be a straight line segment. These are reasonable assumptions since the distance between adjacent crossings is usually very small. Finally, slippage at a crossing is neglected. This is also a reasonable assumption in most cases as reported by Potter [22]. With the above simplifications, a fitting problem can be reduced to a surface-surface intersection problem with appropriate initial conditions. The initial conditions include the starting point for the fit, the initial orientation of the sheet, and the guide lines for the fit [4].

4.1 Fitting as a Surface-Surface Intersection Problem

Let $p(i,j)(0 \leq i \leq M, 0 \leq j \leq N)$ denote a crossing. Given $p(0,j)$ and $p(i,0)$ as a set of guide lines, and given a surface that is represented by a NURBS surface, the problem of obtaining the crossing $p(i,j)$ is formulated as an intersection between two spheres and a NURBS surface as follows:

Sphere 1:

$$(x-x_1)^2+(y-y_1)^2+(z-z_1)^2=(d^{weft})^2, \tag{13}$$

Sphere 2:

$$(x-x_2)^2+(y-y_2)^2+(z-z_2)^2=(d^{warp})^2, \tag{14}$$

NURBS Surface (degree $m \times n$):

$$\mathbf{r}(u,v) = \frac{\sum_{i=0}^{Cu-1}\sum_{j=0}^{Cv-1} w_{i,j}\mathbf{c}_{i,j}N_i^m(u)N_j^n(v)}{\sum_{i=0}^{Cu-1}\sum_{j=0}^{Cv-1} w_{i,j}N_i^m(u)N_j^n(v)}, \tag{15}$$

where $p(i-1,j) = \mathbf{r}(u_{i-1},v_j) = (x_1,y_1,z_1)$, $p(i,j-1) = \mathbf{r}(u_i,v_{j-1}) = (x_2,y_2,z_2)$, C_u is the number of control points along u-axis, and C_v is the number of control points along v-axis. (See Figure 3).

By substituting Equation (15) into Equations (13) and (14) we obtain

$$\left.\begin{array}{rcl} F_1 & \equiv & (x(u,v)-x_1)^2 + (y(u,v)-y_1)^2 \\ & + & (z(u,v)-z_1)^2 - (d^{weft})^2 = 0 \\ F_2 & \equiv & (x(u,v)-x_2)^2 + (y(u,v)-y_2)^2 \\ & + & (z(u,v)-z_2)^2 - (d^{warp})^2 = 0 \end{array}\right\}, \tag{16}$$

where $\mathbf{r}(u,v) = (x(u,v), y(u,v), z(u,v))$.

Equation (16) represents a system of non-linear equations with u and v as variables. Assuming that the given NURBS surface is differentiable, Equation (16) can be solved by the Newton-Raphson method. Let $(u^{(k)}, v^{(k)})$ denote a pair of variables at the k-th iteration. Then the $k+1$-th pair can be obtained by the following formula:

$$\begin{bmatrix} u^{(k+1)} \\ v^{(k+1)} \end{bmatrix} = \begin{bmatrix} u^{(k)} \\ v^{(k)} \end{bmatrix} - \begin{bmatrix} \Delta u^{(k)} \\ \Delta v^{(k)} \end{bmatrix}, \tag{17}$$

where

$$\begin{bmatrix} \Delta u^{(k)} \\ \Delta v^{(k)} \end{bmatrix} = \begin{bmatrix} \frac{\partial F_1}{\partial u} & \frac{\partial F_1}{\partial v} \\ \frac{\partial F_2}{\partial u} & \frac{\partial F_2}{\partial v} \end{bmatrix}^{-1} \begin{bmatrix} F_1(u^{(k)}, v^{(k)}) \\ F_2(u^{(k)}, v^{(k)}) \end{bmatrix}. \tag{18}$$

4.2 Initial Conditions

Initial conditions must be sufficient, but not excessive, in order to uniquely determine the fit between a point on a sheet of cloth in 2D space and the corresponding point on a surface in 3D space. If, for instance, they are over-specified, it is likely that no solution will satisfy the given initial conditions. If, on the other hand, they are under-specified, a unique solution may not be found. We have developed a method for specifying initial conditions illustrated in Figure 4. In 2D space, a guide line is specified by a straight line, although it is not necessarily aligned with any weft or warp thread. A starting point must be chosen somewhere on the guide line, but it is not expected to coincide with a thread crossing. When a guide line is specified as above, *auxiliary crossings* are automatically defined as the intersections between the guide line and threads, which are marked by circles in Figure 4. Refer to [4] for more details on the method of obtaining the fit for auxiliary crossing. The guide line generally subdivides the 2D space into two half-spaces. We define a *sweeping direction* with a 2D vector for each half-space. It is the sweeping direction that determines the order of the mapping calculations among regular mesh points belonging to the half-space.

The result of a fit depends not only on the initial conditions in 2D space, but also on those in 3D space. The biggest difference in the initial conditions between 2D space and 3D space is the specification of the guide line, since the guide line in 3D space is generally a space curve lying on the surface, instead of a straight line in 2D space. When defining a 3D space curve as a guide line, it is important that it be easy to specify and that it should lead to flexible fitting results. We have considered the following methods for specifying the guide line in 3D space: a point sequence, a parametric curve, an intersection curve between the given surface and another surface, and a special space curve.

A point sequence on the given surface is a straightforward way to specify the guide line. If the given surface is complex, however, it may not be easy to obtain such points. A parametric curve can be relatively easy to specify. Examples include an isoparametric curve in which $u = constant$ and $v = constant$. As the parametric curve becomes complex, the specification also becomes complex. A better method may be to specify the guide line as the intersection between two surfaces. For instance, defining the guide line as the intersection between a plane and the given surface may be in most practical cases satisfactory [4].

Another method for specifying the guide line is to define it as a special curve by considering local differential geometry around the starting point of a fit. Such curves may include: (1) lines of curvature passing through the

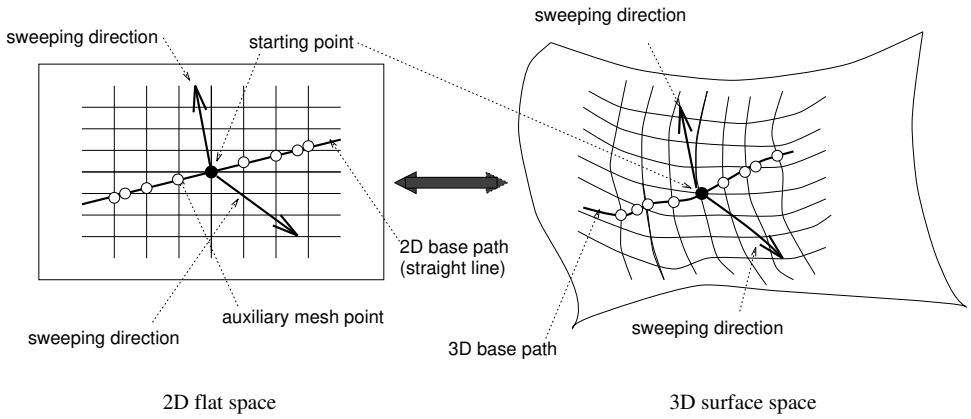

Figure 4: Initial conditions.

starting point and (2) geodesics passing through the starting point [9, 31]. It is well-known that lines of curvature passing through a point are determined intrinsically and uniquely except at an umbilic point [9, 31]. Moreover, for a non-umbilic point, two lines of curvature are always perpendicular to each other. We may reduce the distortion along the guide line by taking advantage of this feature. On the other hand, if we define the guide line as a geodesic, we may obtain a fit with the smallest amount of woven cloth materials because a geodesic has the shortest length between two points on the surface [9, 31]. Furthermore, since the base path is not distorted, according to Lemma 2, the deformation energy accumulated along the path can be minimized.

Example: We consider a fit to an octant of a sphere with radius R. We assume that the geometry is defined in the first octant ($X \geq 0$, $Y \geq 0$, $Z \geq 0$). Experiments with three different initial conditions have been carried out, which are summarized in Table 1. Specifically, they have a common guide line along the circle on the $Y = 0$ plane in 3D space, and the mesh size of the ply is assumed to be 40×40. In 2D space, cases (a) and (b) have a guide line parallel to the weft threads, and case (c) has a guide line at a 45 degree angle to both the wefts and the warps. The starting point is denoted by P_s, and the sweeping directions are denoted by directed arrows incident from the starting point. Figure 5 shows three fitting results and Figure 6 shows the 2D plane development patterns for the corresponding fittings. Note that the bold line segments in the 2D plane developments represent the area used for the fittings. Figure 7 shows the same result, with colors assigned based on the thread angle values ($T \equiv \gamma$ in Figure 7).

In order to compare the results, we calculated the following values, which are listed in Table 2: (1) the area of the 2D sheet fitted to the surface, (2) the maximum and minimum thread angles, and (3) the shear deformation energy. The area of the sheet is approximated by summing up the number of crossings in the 2D plane development pattern. The maximum (γ_{max}) and minimum (γ_{min}) thread angles are simply calculated as $\gamma_{max} = max(\gamma_{i,j})$ and $\gamma_{min} = min(\gamma_{i,j})$, where $\gamma_{i,j} = \arccos(\mathbf{r_i} \cdot \mathbf{r_j})$, and $\mathbf{r_i}$ is the unit weft vector and $\mathbf{r_j}$ is the unit warp vector at a crossing $p(i, j)$. The shear deformation energy is approximated by the value $\sum_{i,j} \cos^2 \gamma_{i,j}$ [34].

Given the values in Table 2, we may evaluate the quality of the fittings. The best fit is the one that consumes the smallest area in 2D space, has the least variation of the thread angles (i.e. minimum γ_{max} and maximum γ_{min}), and has the minimum deformation energy. It should be noted, however, a "best" fit may not be unique. In our simulation experiments, the best fit among the three is case (b). This can be visually confirmed by Figure 7; case (b) has only green colors, whereas cases (a) and (c) have yellow and red colors indicating the large shear deformation. Figure 8 shows the fitting results with an actual sheet of woven cloth fiberglass, corresponding to the fittings in Figure 5. It is noteworthy that the theoretical deformation patterns that we have predicted match quite nicely with the real deformation patterns.

Next we present several fittings onto one third of a surface of revolution. Figure 9 presents the results of six different fittings. The first three cases ((a), (b), and (c)) have a common base path along the boundary curve on the $Y = 0$ plane, and the last three cases ((d), (e), and (f)) have a common base path along the curve on the $X = Y$ plane. In 2D space, cases (a), (c), (d), and (f) have the base path parallel to the warps, and cases (b) and (e) have the base path at a 45 degree angle to the warps. The definition of the sweeping directions and the starting points is similar to the previous example, and the initial conditions are summarized in Table 3. We assume that the mesh size of the 2D

	(a)	(b)	(c)
3D			
starting point	(0,0,R)	($\frac{R}{2}$,0,$\frac{R}{2}$)	(0,0,R)
sweeping direction	(0,1,0)	(0,1,0)	(0,1,0)
base path	Y = 0	Y = 0	Y = 0
2D			
starting point	(0,0)	(20,0)	(15,0)
sweeping direction	(0,1)	(0,1)	(-1,1)
base path	Y = 0	X = 20	Y = X - 15

Table 1: Initial conditions for the three fitting in Figure 5.

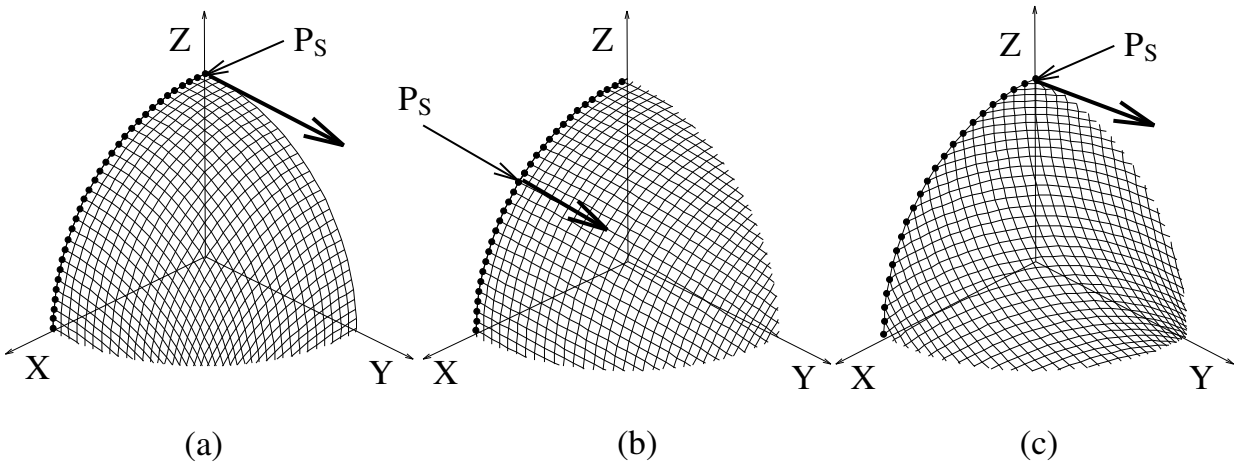

Figure 5: Three fittings to an octant of a sphere.

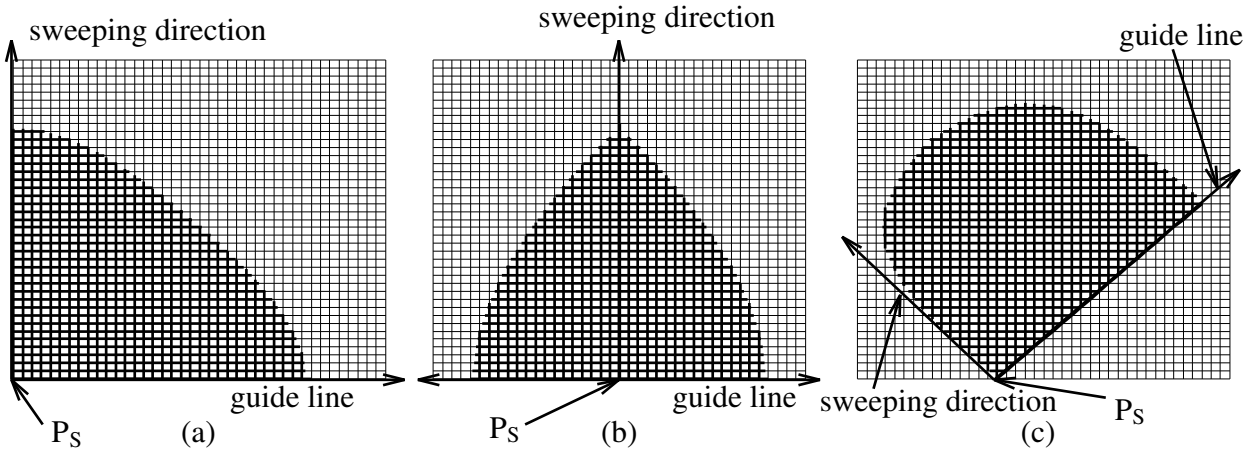

Figure 6: 2D plane development patterns.

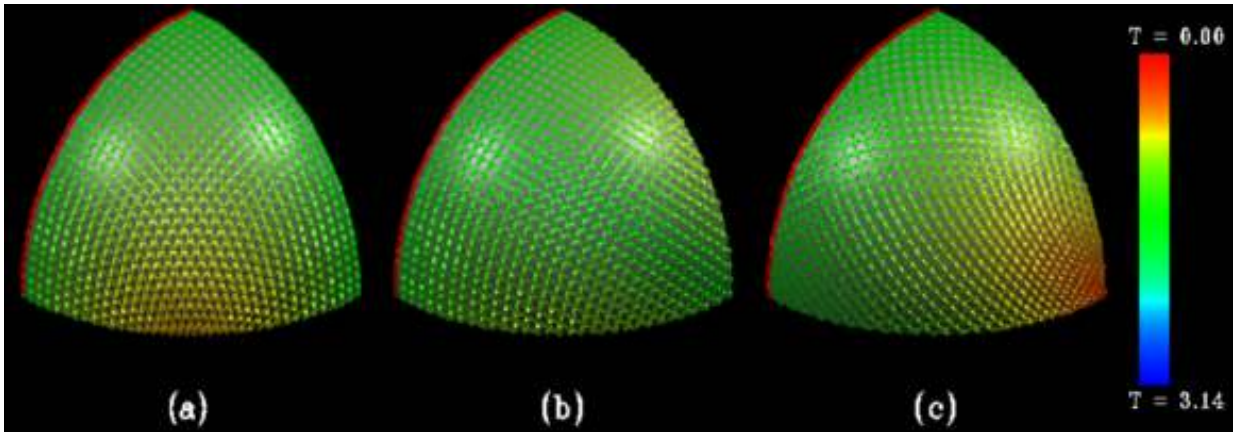

Figure 7: Fittings to an octant of a sphere with colors assigned, based on the thread angle values (T).

Figure 8: Fitting results with an actual sheet of woven cloth fiberglass

	(a)	(b)	(c)
area	716	657	725
$\min(\arccos \gamma_{i,j})$	0.707	1.167	0.353
$\max(\arccos \gamma_{i,j})$	1.570	1.570	1.570
$\sum_{i,j}(\cos \gamma_{i,j})^2$	82.5	17.4	128.2
$100 \times B(i,j)$	0.119	0.091	0.099

Table 2: Comparison of results with different initial conditions.

	(a)	(b)	(c)
3D			
starting point	(10,0,0)	(10,0,0)	$(\frac{55}{8},0,\frac{15}{2})$
sweeping directions	(0,1,0)	(0,1,0)	(0,1,0)
base path	Y = 0	Y = 0	Y = 0
2D			
starting point	(0,0)	(0,30)	(0,20)
sweeping directions	(1,0)	(1,-1)	(1,0)
base path	X = 0	Y = X + 30	X = 0

	(d)	(e)	(f)
3D			
starting point	$(10,10\sqrt{3},0)$	$(\frac{55}{8},\frac{55}{8}\sqrt{3},\frac{15}{2})$	$(\frac{55}{8},\frac{55}{8}\sqrt{3},\frac{15}{2})$
sweeping directions	(1,-1,0)	(1,-1,0)	(1,-1,0)
	(-1,1,0)	(-1,1,0)	(-1,1,0)
base path	X = Y	X = Y	X = Y
2D			
starting point	(35,0)	(35,35)	(35,35)
sweeping directions	(-1,0)	(-1,1)	(-1,0)
	(1,0)	(1,-1)	(1,0)
base path	X = 35	Y = X	X = 35

Table 3: Initial conditions for the fitting in Figure 9.

ply is 70 $\times$ 70. Figure 10 includes the 2D plane developments corresponding to the fittings in Figure 9.

Figures 9 and 10 clearly demonstrate the critical effect of initial conditions on the final mappings. Table 4 summarizes the results of the six different cases. Case (f) requires the smallest ply area. Case (d) has the minimum γ_{max}, and case (f) has the maximum γ_{min}. Case (d) has the least shear deformation energy, and case (e) has the least bending deformation energy. We cannot conclude which is the best fitting, but we can clearly state that cases (d), (e), and (f) produce better results than cases (a), (b), and (c). In the six different results, case (c) is exceptional since it fails to cover the entire surface region with the given 2D ply.

	(a)	(b)	(c)	(d)	(e)	(f)
area	1159	1246	1474	1023	1017	1010
$\min(\arccos\gamma_{i,j})$	0.719	1.266	1.347	1.157	1.252	1.347
$\max(\arccos\gamma_{i,j})$	2.832	2.764	3.135	2.182	2.317	2.429
$\sum_{i,j}(\cos\gamma_{i,j})^2$	211.5	385.9	588.6	36.7	50.5	40.9
$100 \times B(i,j)$	0.052	0.068	0.042	0.055	0.024	0.048

Table 4: Comparison of results with different initial conditions.

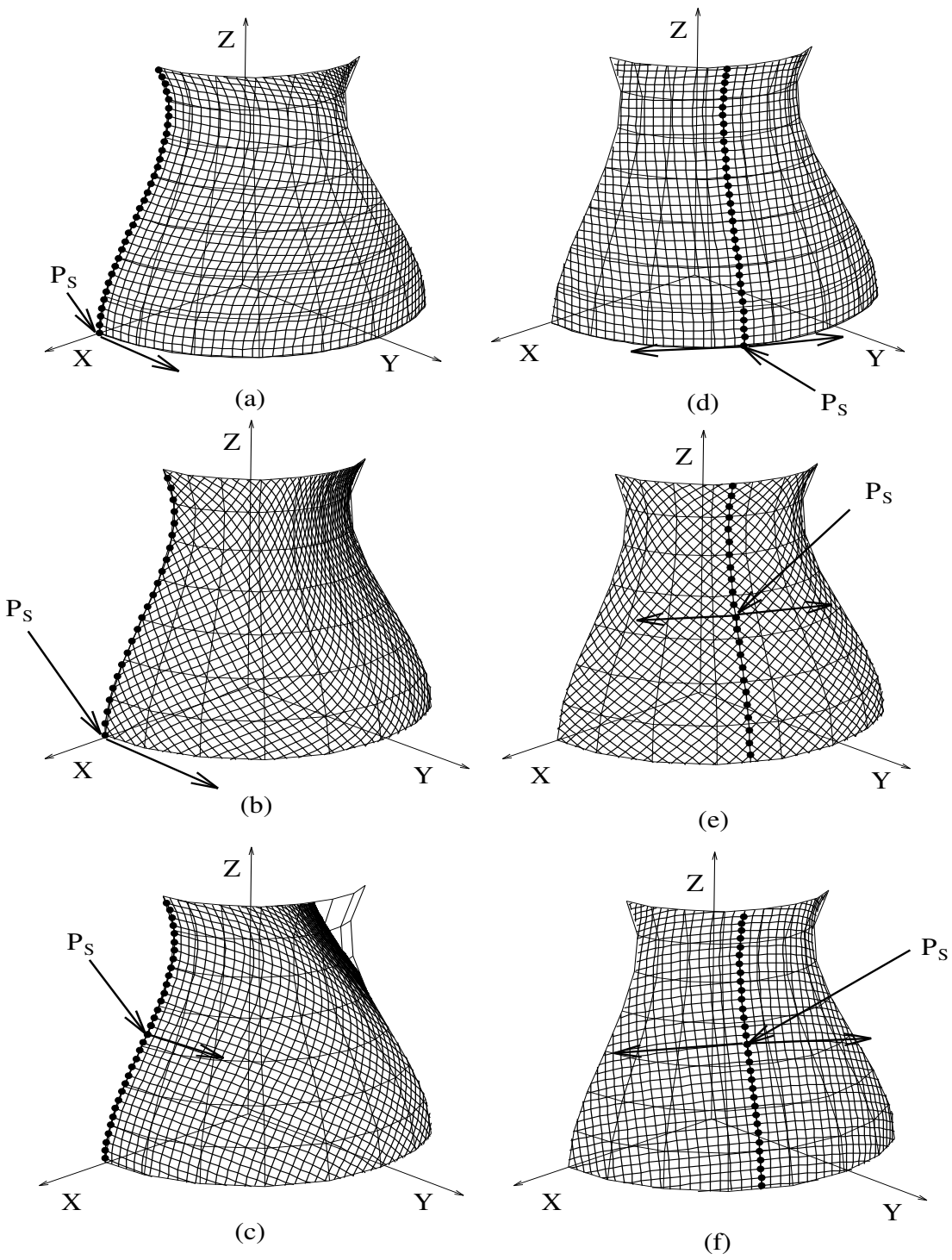

Figure 9: Fittings to a third part of a surface of revolution with six different initial conditions.

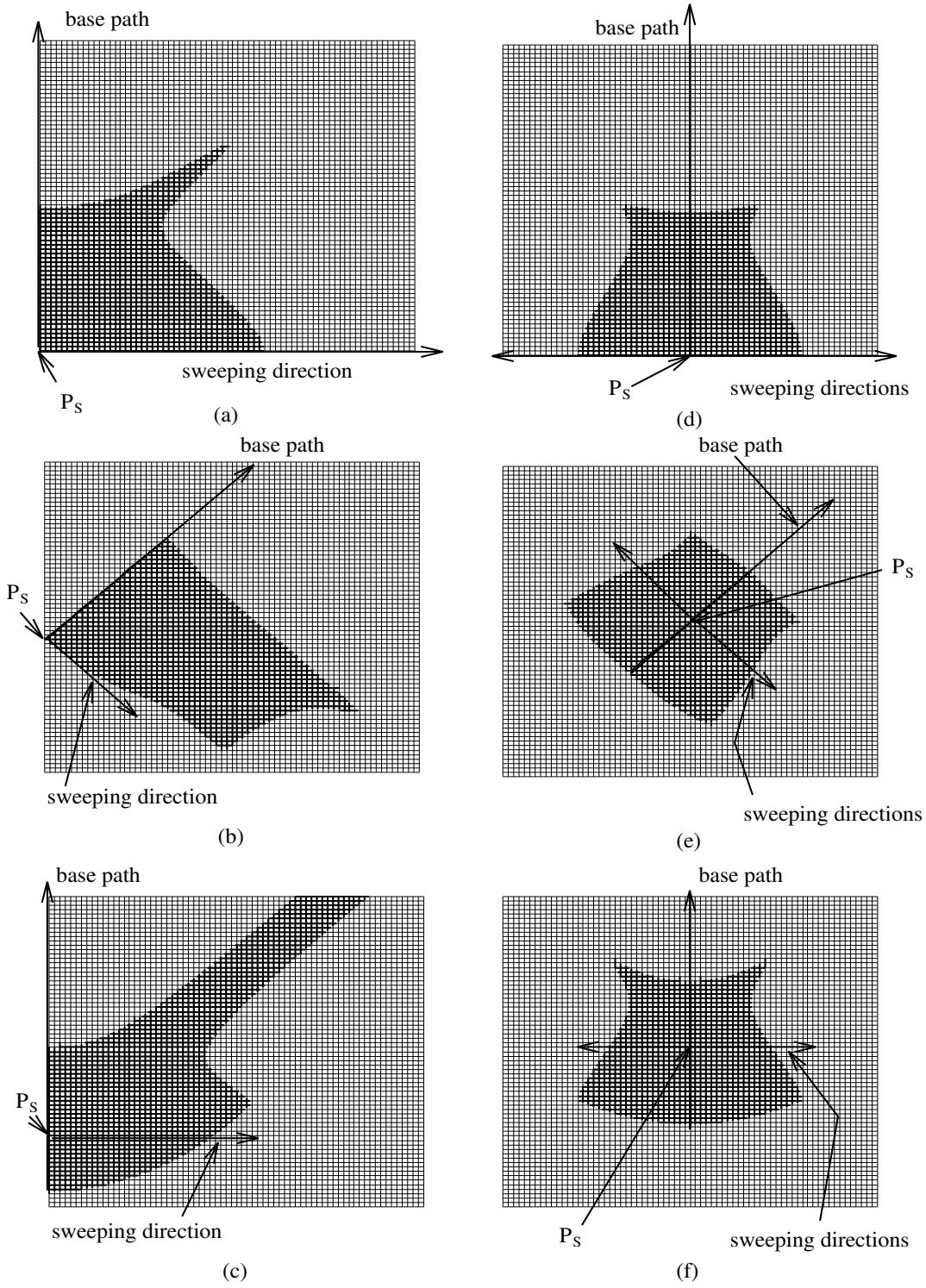

Figure 10: Plane development patterns used for the fitting to a third of a surface of revolution.

5 Predicting the Goodness of a Fit

Here we will introduce mathematical tools for evaluating the goodness of a fit. Let I_K denote a Gaussian curvature integral over an entire surface region as follows:

$$I_K = \int\int K \, dS. \tag{19}$$

Since I_K provides an "intrinsic" quantity, it does not depend upon either the surface coordinate system or the Tchebychev net coordinate system. On the other hand, as we have observed in the previous section, the fitting result depends heavily upon the initial conditions. In order to capture this phenomenon, we define a *path-dependent Gaussian curvature integral* ($I_{K_{i,j}}$) over a surface region as follows:

$$I_{K_{i,j}} = \int_{x_0}^{x_i} \int_{y_0}^{y_j} K_{x,y} \, dxdy, \tag{20}$$

where the starting point is specified at (x_0, y_0) in 2D space. Clearly, $I_{K_{i,j}}$ in Equation (20) depends upon how we have swept the sheet so far from the starting point (x_0, y_0) to the current point (x_i, y_j) on the surface region.

In particular, if the guide line is aligned with $X = 0$ thread (or alternatively $Y = 0$ thread), and the sweeping direction is in the positive Y direction (or in the positive X direction), $I_{K_{i,j}}$ is approximated by the following formula:

$$I_{K_{i,j}} \approx \sum_{p=1}^{i} \sum_{q=1}^{j} K_{p,q} \Delta x \Delta y, \tag{21}$$

where Δx and Δy represent the distances between adjacent wefts and warps, respectively, and are constants due to the inextensibility of the threads of a Tchebychev net. From Equation (21), we can derive an interesting recursion formula regarding the path-dependent Gaussian curvature integrals as follows:

$$I_{K_{i,j}} = I_{K_{i-1,j}} + I_{K_{i,j-1}} - I_{K_{i-1,j-1}} + K_{i,j} \Delta x \Delta y, \tag{22}$$

where $I_{K_{0,j}} = I_{K_{i,0}} = 0$. This can be easily proved by induction on i and j for $i \geq 1$ and $j \geq 1$.

Example: Let $\Delta x = \Delta y = d$. Consider an octant of a sphere. Since the Gaussian curvature of a sphere is constant, $I_{K_{i,j}}$ is obtained from Equation (22) as a closed formula as follows:

$$I_{K_{i,j}} = ij(\frac{d}{R})^2. \tag{23}$$

This is a monotonically increasing function with the surface region area proportional to $i \times j$. Figure 11 shows the surface region that must be integrated at the point **P** where the path-dependent Gaussian curvature integral becomes maximum for each of the fittings in Figure 5. Clearly, point **P** in case (c) needs the largest area for the path-dependent Gaussian curvature integral. Therefore, the thread angle at **P** in case (c) must be minimum. This conforms to the result obtained in Figure 5.

6 Preventing Anomalies in Broadcloth Composites

Many anomalous events, or manufacturing faults, may occur during the lamination process, e.g., wrinked layers, voids, incorrect fiber orientations, delaminations, and resin starved/rich regions. We have focused on developing techniques for detecting and preventing two kinds of anomalies, wrinkles and voids, during design. Both of these anomalies may occur when thread angles rotate beyond their deformation limits (i.e. locking angle). In other words, as long as the thread angle stays between certain minimum and maximum values, the ply behaves acceptably. Additionally, problems occur when the ply cannot fit to a given surface because of the local high convexity or concavity . If there is local high convexity, the resulting state is called "breaking", and if there is local high concavity, it is called "bridging".

We propose three different approaches for preventing anomalous events. In the first approach a good initial path specification is automatically calculated given the input surface shapes and a ply material. This may be done by

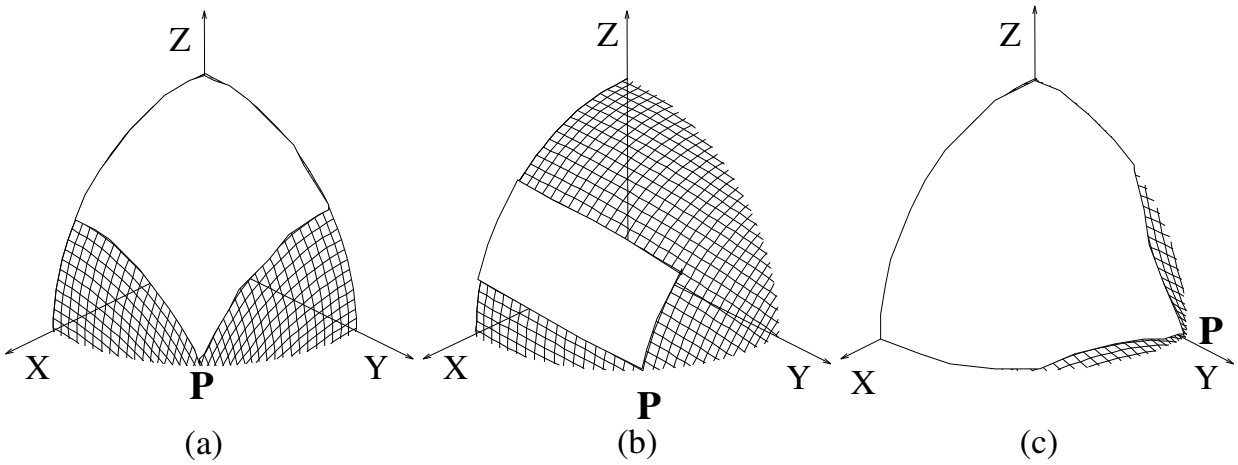

Figure 11: Surface region filled in white represents the region that must be integrated to obtain the path-dependent Gaussian curvature integral at point **P** in each case.

considering local surface differential geometry properties such as the distribution of Gaussian curvatures. The second approach involves trimming and splitting the ply into pieces whenever anomalous events may occur. For the wrinkling case, this splitting corresponds to "darting" the excessive portion. For the breaking and bridging cases, it corresponds to "cutting" the cloth and "patching" the necessary portion. In the final approach the actual underlying surface is modified in order to remove areas of high cloth deformation.

6.1 An Algorithm for Finding a Good Initial Path

Anomalous events such as wrinkling and tearing are very sensitive to the initial conditions of the fitting process. Good initial paths may greatly decrease the possibility of anomalous events. Lemmas 1 and 2 lead to an algorithm for finding a good initial path that produces an optimal fitting result, given a 3D surface shape. Due to Lemma 1, if we start fitting at a point on the surface where the absolute value of the Gaussian curvature is the largest, we can maximize the minimum thread angle or minimize the maximum thread angle in the fitting. This is because no location other than the starting point has a larger Gaussian curvature, and thus the change in the thread angle will be smaller than the cases starting at other points. Similarly, due to Lemma 2, if we align the initial path (e.g. base path) with a geodesic on the surface, we can keep the angular relationship between wefts and warps along the path. By taking advantage of these Lemmas, we can potentially suppress the accumulation of the strain energy caused by shear deformation, if we judiciously set up the starting point and the initial base path. In addition, it is generally true that the starting point should be located around the center of the surface region if there is no unique point which has the maximum Gaussian curvature. The validity of this comes from the observation that the deformation of a Tchebychev net caused by changing thread angles tends to be amplified as the fitting proceeds toward the boundary of the surface region. We thus add this observation to our algorithm as a heuristic rule. Intuitively, this rule can be interpreted as minimizing the maximum distance from the starting point.

These considerations lead to an algorithm that provides a reasonably good initial path that may potentially minimize the total deformation energy.

1. Find a point in a given surface region where the absolute value of the Gaussian curvature ($|K|$) is maximum. If there are two or more points with the same maximum, choose the one closer to the center of the surface region.
2. Calculate principal directions there and align the base path with one of the principal directions corresponding to $\kappa_n = \kappa_{max}$, where κ_n is the normal curvature, and κ_{max} is the maximum value of κ_n at the point.
3. Set up the base path along a geodesic on the surface region, having the initial direction specified by $\kappa_n = \kappa_{max}$.

In Step 1, note that in order to determine the point closest to the center of a surface region, we need a measure of the distance. Mathematically, the distance between a point of interest in a surface region and a point on the boundary

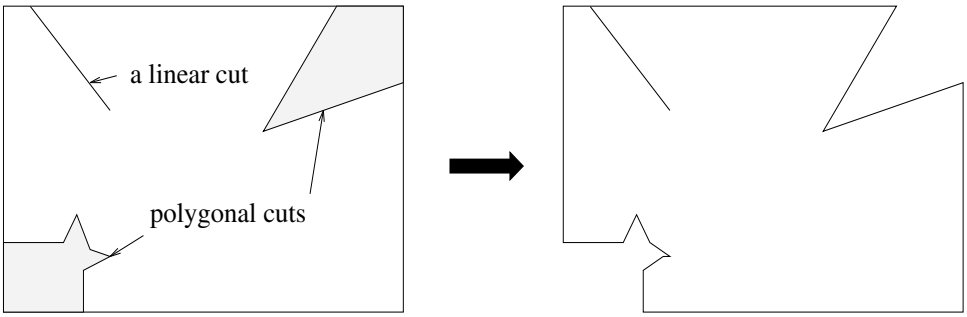

Figure 12: Trimmed darts (before and after insertions)

is defined as the arc length along the geodesic passing through the two points. However, it is not necessary to find the exact point closest to the center of a surface region since candidate points themselves are selected by "sampling" (or "approximation"). Assuming the surface region is convex in a bivariate parametric space of the surface, we may select the point closest to the center by checking the distance between (u, v) and $(\frac{u_{min}+u_{max}}{2}, \frac{v_{min}+v_{max}}{2})$, where (u, v) is the coordinate of the point of interest and (u_{min}, v_{min}) and (u_{max}, v_{max}) are the minimum and maximum parametric values for the surface. The computation of Gaussian curvature, principal directions, and geodesics are detailed in [3].

6.2 Dart Insertion for Preventing Anomalies

In regions where excessive or insufficient material will cause anomalous events such as gaps and wrinkles, a "dart" may be inserted in the broadcloth. These modifications to the cloth relieve the extreme shearing which ultimately produce defects in the final laminated part. Our work in dart insertion has been detailed elsewhere[5]. A brief summary with results is included here for completeness.

6.2.1 Models for Darts

We have experimented with a variety of darts and have found that *trimmed darts* are the most effective. Trimmed darts simply remove excessive materials without attempting to stitch the new edges together. Trimmed darts are further classified into two types according to the shape of the trimmed materials. If the shape is given by an arbitrary polygon, the trimmed dart is called a *polygonal cut*. If, on the other hand, the shape is given by a linear line segment, it is called a *linear cut*. Figure 12 shows two polygonal cuts and a linear cut. Note that our underlying inextensibility assumption is kept valid under the insertion of darts. The distance and topology between adjacent mesh points, however, may be affected by the insertion of a dart.

6.2.2 Strategies for Dart Insertion

There are two issues related to dart insertion: (1) location of the dart, and (2) shape of the dart. The solution to the problem of dart location becomes tractable if we limit our attention to anomalous events caused by excessive shear deformation. With this limitation, the problem can now be rephrased as one of identifying regions of excessive shear deformation. In essence, darts should be inserted where excessive shear deformation is likely to occur, under the given initial conditions. We hereafter refer to such a region as a *critical region*. Critical regions are classified into two types: (1) *lower critical regions*, in which the thread angle of every mesh point is less than γ_{min} and (2) *upper critical regions*, in which the thread angle of every mesh point is greater than γ_{max}.

The optimal dart shape is one that removes all critical regions with the simplest shape. Another optimality criterion may include the ease of inserting darts. In order to find the optimal shape, we employ a strategy based on a relaxation technique. We start with a dart of a certain shape that includes a part (or all) of the critical region. Then, we incrementally modify the shape so that at each step we decrease the critical region until none is left.

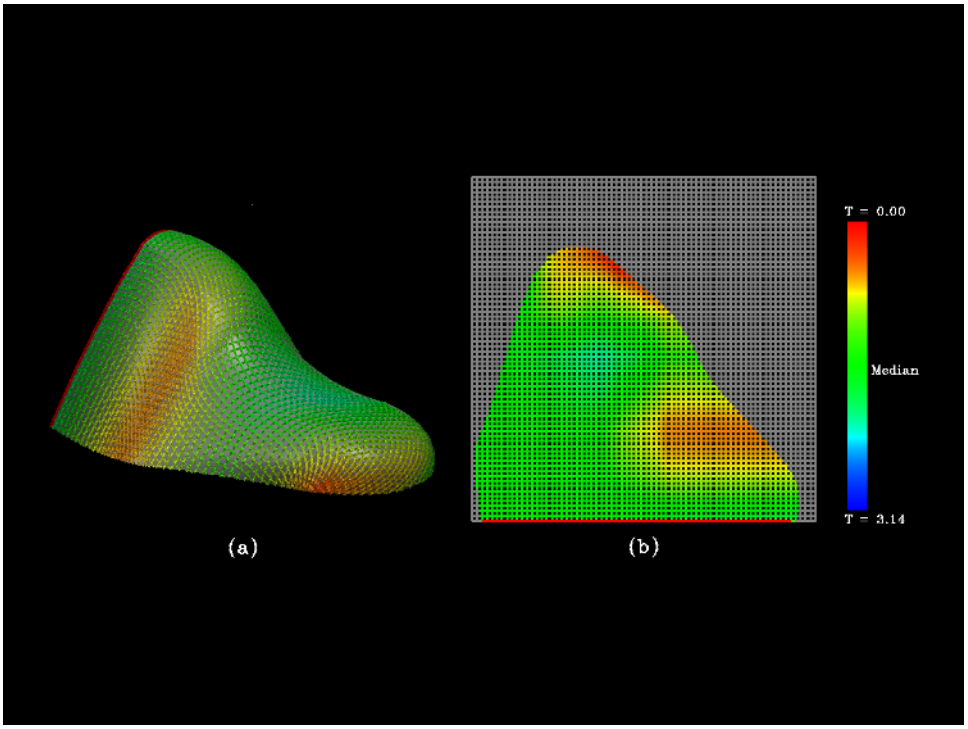

Figure 13: (a) A fitting to a shoe-like object with colors based on the thread angle values at each mesh point, and (b) the 2-D plane development

6.2.3 Overlap Removal Algorithms

Overlaps may occur in the fitting result when a linear cut is inserted into a lower critical region. Our goal is to remove major overlaps and find the optimal shape for a dart that is to be inserted into a lower critical region. The algorithm for removing overlaps includes two major steps: (1) finding overlaps and (2) updating the shape of the dart. Assuming that both the 2-D and the 3-D deformed woven cloth composites are approximated by a collection of triangles, overlaps in the fitting result may be found with a point-triangle location algorithm in 3-D space. Specifically, every mesh point is tested for inclusion in each triangle in 3-D space. An overlap is identified if the projection of the mesh point 'P' onto the plane formed by three mesh points, A, B, and C, is located inside triangle ABC.

Once overlaps are found, we remove them and update the shape of the dart. The removal of an overlapping mesh point is called *safe* if it does not open a gap whose size is larger than the distance between adjacent mesh points. In other words, if an overlapping mesh point lies on the border of the actual shape of the material, then its removal is "safe." A number of methods may be used to remove overlapping mesh points. These produce a variety of valid mesh configurations based on the different sequences utilized to select and remove mesh points. It is therefore necessary to resort to a particular optimizing strategy during overlap removal. The optimization criteria that we use include the following alternatives: 1) minimize the shear deformation in the resulting woven cloth, 2) minimize the raggedness of the darting edge, and 3) increase the symmetry along the cut.

It may not be possible to implement an algorithm that satisfies all of the above optimizing criteria simultaneously. For this reason, we have implemented several different algorithms to correctly remove overlaps. The following is a list of the methods that we have implemented. The choice of method depends on what optimization criterion is considered most important for the current configuration.

- **Sequential Method:**
  The first mesh point in the overlapping point list (OPL) is tested to determine if it can be safely removed.
- **Random Method:**

Randomly select a mesh point from the OPL and test it to determine if it can be safely removed.

- **Cut Distance Priority Method:**
  The OPL is sorted according to the distance from the cut inserted. The mesh point closest to the cut is tested for safe removal.
- **Thread Angle Priority Method:**
  The OPL is sorted according to the values of thread angles (γ). The mesh point whose $\cos\gamma$ is largest is tested for safe removal.

6.2.4 Examples

Here we describe the fitting of a 2-D ply of woven cloth composites to a surface modeled by NURBS (Non-Uniform Rational B-Spline) surfaces [12], which requirs dart insertion. This example involves fitting a broadcloth ply to a shoe-like object. Figures 13 (a) and (b) show the fitting result and the 2-D plane development pattern, respectively. Two isolated critical regions are clearly visible. Some thread angles in these regions become less than the allowable minimum (γ_{min}), and therefore they are classified as lower critical regions. In order to intuitively identify the critical regions, we shade each mesh point a different color according to its thread angle value. In Figure 13, the variable T attached to the color bar represents the thread angle γ, and the lower critical region is colored red. In addition, the red line in Figures 13 (b) represents the base path for the fitting.

Note that we have assigned colors as follows: red is assigned when $\gamma = 0$ degrees, green is assigned when $\gamma = 90$ degrees, blue is assigned when $\gamma = 180$ degrees, and an interpolated color is assigned in hue space[26] for intermediate values of γ. With this rule, a mesh point takes on a reddish color when γ becomes lower than approximately 30 degrees, which allows us to visually interpret the point as lying in a lower critical region. Although we can shift the color distribution for fine tuning, the above rule is reasonable, since most commercial fabrics "lock" or "jam" at angles less than 35 degrees [18].

In order to remove these critical regions and avoid anomalous events, we insert a trimmed dart. We first insert two linear cuts into the critical regions, as shown in Figure 14 (a), and obtain the fitting result shown in Figure 15 (a). It is interesting that with the insertion of the linear cuts, the part of the critical regions with reddish colors vanishes. Overlaps are observed in the fitting result in Figure 15 (a). We tested three methods for removing the overlaps: (1) the sequential method (Figure 14 (b) for the final shape of the dart and Figure 15 (b) for the fitting result), (2) the cut distance priority method (Figures 14 (c) and 15 (c)), and (3) the thread angle priority method (Figure 14 (d) and 15 (d)). In terms of thread angle values, method (3) produces the best result. In terms of raggedness, methods (1) and (2) produce better results than method (3). In terms of symmetry with respect to the linear cuts, method (2) produces the best result.

6.3 Surface Shape Modification

There are instances where designers have the freedom to modify the shape of the 3D part in order to accomodate the composite lamination process. Here, optimization methods may be used to adjust the surface parameters to produce a broadcloth fitting with minimal deformation.

6.3.1 Algorithm Requirements

The integral Gaussian curvature, I_K, defined in Equation (19) provides a measure for global conformability of a woven cloth composite sheet to a given surface. For example, if $|I_K|$ is less than $\frac{\pi}{2}$, we can globally clothe the surface due to Samelson's theorem (Theorem 2), and if $|I_K|$ is greater than 2π, we cannot globally clothe the surface due to Hazzidakis' theorem (Theorem 1). Given two different surfaces S_1 and S_2 with their $|I_K|$ values denoted by $|I_{K_1}|$ and $|I_{K_2}|$, let us call the shape S_1 *simpler with respect to global conformability* if $|I_{K_1}| < |I_{K_2}|$. In general, the excessive shear deformation that leads to anomalous events is less likely to occur on the surface with a smaller $|I_K|$ value. In particular, if $I_K = 0$ or the surface is a developable surface, no shear deformation will result. Our aim is to investigate shape modifications that satisfy the following requirements:

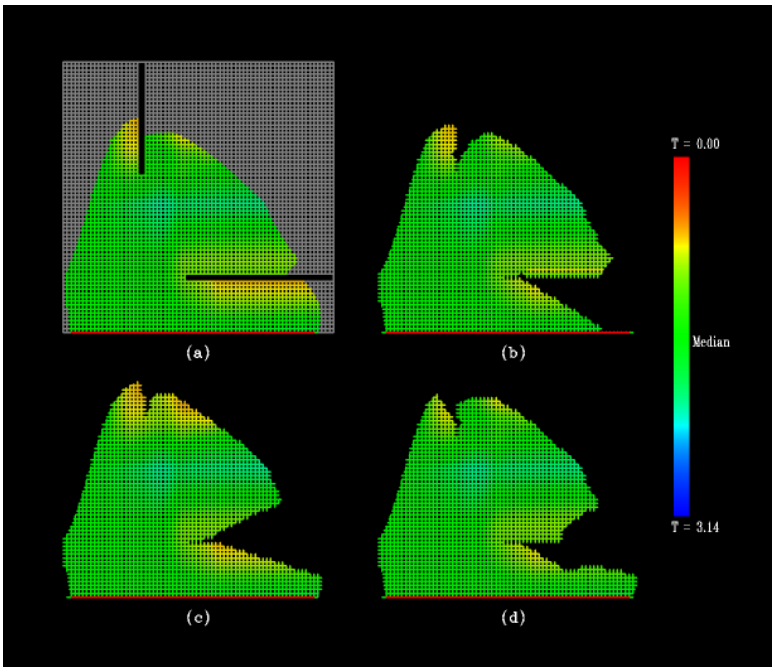

Figure 14: 2-D plane development patterns with trimmed darts: (a) insertion of two linear cuts, (b) polygonal cuts obtained by the sequential method, (c) polygonal cuts obtained by the cut distance priority method, and (d) polygonal cuts obtained by the thread angle priority method

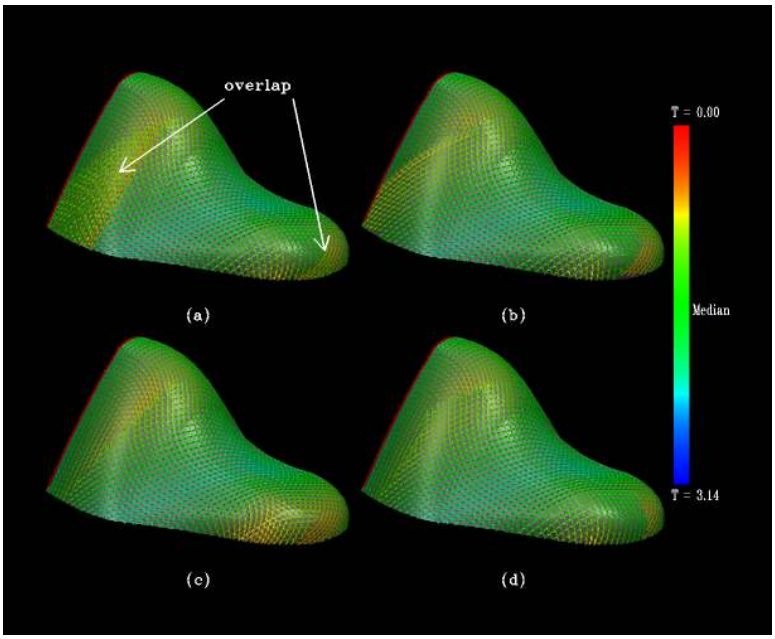

Figure 15: 3-D fitting results with trimmed darts: (a) insertion of two linear cuts, (b) polygonal cuts obtained by the sequential method, (c) polygonal cuts obtained by the cut distance priority method, and (d) polygonal cuts obtained by the thread angle priority method

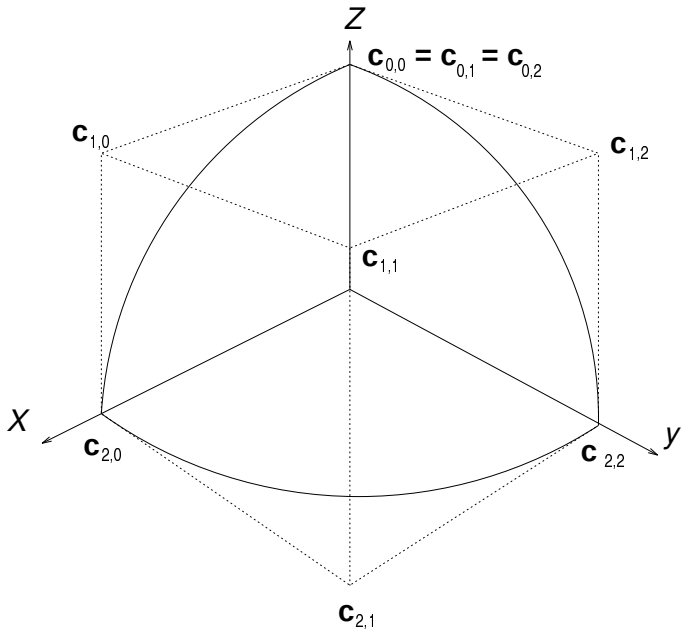

Figure 16: The original shape of an octant of a sphere defined by a rational biquadratic B-spline surface.

1. The integral Gaussian curvature of the modified shape should become less than the original value.
2. The deviation of the modified shape from the original should be kept to a minimum.

Let $I_{K'}$ denote the integral Gaussian curvature of the modified shape. The first requirement then is expressed as $|I_{K'}| < |I_K|$. Similarly, let $\mathbf{r}'(u,v)$ denote a parametric representation of the modified shape. Then, the second requirement is expressed as minimizing the following value:

$$\int_u \int_v ||\mathbf{r}(u,v) - \mathbf{r}'(u,v)||^2 dudv. \tag{24}$$

6.3.2 Modifying a Surface Shape by Editing Control Parameters Interactively

Suppose that a surface is represented by a NURBS surface as in Equation (15). Then, a simple and straightforward approach to modifying the surface shape is to interactively control the parameters that define the NURBS surface. The parameters include “control points”, “knot vectors”, and “weights” of the control points. Editing control points or knot vectors is a straightforward way of modifying the surface shape. The advantage of this method is ease of implementation and ease of specifying the parameters. In order to meet the first requirement, we modify some of the control parameters such that $|I_{K'}| < |I_K|$. However, this is not a trivial task, except when the surface shape is simple enough for us to easily infer the Gaussian curvature at every point on the surface. This is true because the Gaussian curvature of a surface is very sensitive to minute changes in the surface [6]. With the similar reasoning, it is also difficult to meet the second requirement.

6.3.3 Modifying a Surface Shape by Finding Optimal Weights Automatically

A better method for satisfying the requirements of shape modification may be to modify the weights of the control points, while keeping the control points and knot vectors unchanged. This ensures that, as long as the new weights remain positive, the modified shape will lie within the convex hull defined by the original control polygon [12]. Thus, the problem is converted into an unconstrained optimization problem as follows: find a set of weights $\mathbf{w} = \{w_{i,j}\}$ for a given NURBS surface, $\mathbf{r}(u,v)$, that satisfy

$$G(\mathbf{w}) = |\int_u \int_v K(u,v;\mathbf{w}) dudv| - \delta = 0, \tag{25}$$

where δ denotes a threshold value, satisfying $\delta \equiv |I_{K'}| < |I_K|$. The solution to Equation (25) only meets the first requirement. The second requirement may be satisfied by adding the constraint that the deviation, $D(\mathbf{w})$, should be minimum, where

$$D(\mathbf{w}) = \int_u \int_v ||\mathbf{r}(u,v;\mathbf{w}_0) - \mathbf{r}(u,v;\mathbf{w})||^2 du dv \tag{26}$$

and $\mathbf{w}_0$ denotes the original weights for the NURBS surface. From Equation (25) and the constraint given by Equation (26), the shape modification problem is translated into a constrained optimization problem [13] as follows: minimize $D(\mathbf{w})$ with the constraint that $G(\mathbf{w}) = 0$. A function $F(\mathbf{w}, \lambda)$ is defined as follows:

$$F(\mathbf{w}, \lambda) = D(\mathbf{w}) + \lambda G(\mathbf{w}), \tag{27}$$

where λ denotes an arbitrary variable. $F(\mathbf{w}, \lambda)$ is at a local minimum when its gradient vector is zero [13], i.e.,

$$\nabla F(\mathbf{w}, \lambda) = 0. \tag{28}$$

Example: Consider an octant of a sphere again. Let $\delta = \pi/4$. Figure 16 illustrates an octant of a sphere defined by a rational biquadratic B-spline surface. The control points and the associated weights are denoted by $\mathbf{c}_{i,j}$ and $w_{i,j}$, respectively, for $0 \leq i \leq 2$ and $0 \leq j \leq 2$. The knot vector in the u direction is $\{0, 0, 1, 1\}$ and the knot vector in the v direction is $\{0, 0, 1, 1\}$.

It should be noted that, in general, as the number of weights to be selected for shape optimization increases, the number of solutions that satisfy Equation (25) increases. Figure 17 shows some of our experimental results. Figure 17 (a) shows the original shape of the octant of a sphere. Figure 17 (b) corresponds to the result obtained by selecting the weight $w_{2,1}$ and modifying it using Equation (25). Figure 17 (c) is obtained by modifying three weights $w_{1,0}$,$w_{1,2}$, and $w_{1,1}$ with Equation (25). In Figure 17 (d), two weights $w_{1,1}$ and $w_{2,1}$ are selected and the constrained optimization with Equation (28) is performed. Note that the edges of the control polygon in Figure 17 are shaded with colors. Specifically, a green color is assigned to the weight value 1.0. As the weight value becomes large, the color shifts toward red. Similarly, as the weight value becomes small, the color shifts toward blue.

To compare the results in terms of the deviation from the original shape, we have assigned colors based on the deviation value from the original shape at each (u, v) point on the modified surface. Figure 18 shows the deviations with colors, corresponding to the examples of Figure 17. Red colors are assigned to areas of large deviation values, and green colors are assigned to areas of no deviation values. Clearly, Figure 18 (d) has the minimum deviation among the three cases ((b), (c), and (d)). Figure 19 demonstrates the distribution of Gaussian curvatures with colors for the same examples. Here, colors are assigned as shown in the color bar. Since the original spherical shape has a constant positive Gaussian curvature, Figure 19 (a) has a yellow color everywhere. The shapes corresponding to cases (b) and (c) have bumps on the surface where Gaussian curvatures take relatively large values. The optimal shape, case (d), looks similar to case (a) in Figure 17, but it has a somewhat flatter region in the middle, as depicted by the green colors in Figure 19 (d). Figure 20 contains the fitting results for each shape with colors based on the thread angle values. Initial conditions for the fittings are the same as those in case (c) in Figure 5. It should be noted that the fitting results after shape modification include no "reddish" regions that are susceptible to anomalous events.

7 Conclusion and Discussion

We have presented a Tchebychev net cloth model and described the method for simulating a fit of a sheet of woven cloth composites to an arbitrary curved surface. Two algorithms were presented: (1) a numerical algorithm that solves the mathematical formula of the Tchebychev net using a finite difference method, and (2) an algorithm that solves the fitting problem by reducing the original problem to a surface-surface intersection problem. It has been shown that the Gaussian curvature integral plays an important role for estimating the goodness of a fit.

We have proposed three approaches to the problem of preventing anomalous events such as wrinkles and breaks that may occur during the fitting process. In the first approach a good initial path specification is automatically calculated given the input surface shapes and a ply material. This may be done by considering local surface differential geometry properties such as the distribution of Gaussian curvatures. The second approach involves trimming and splitting the ply into pieces whenever anomalous events may occur. For the wrinkling case, this splitting corresponds

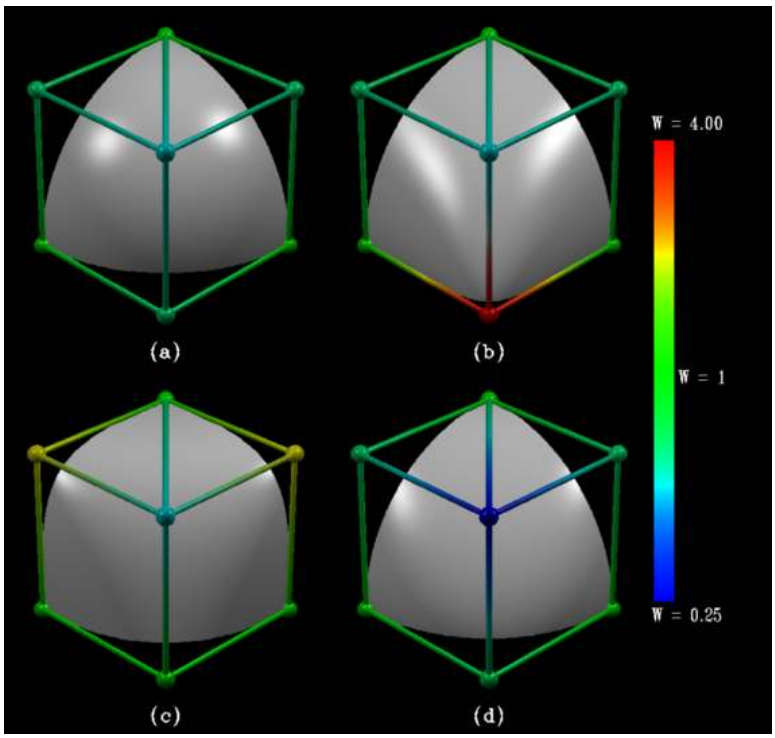

Figure 17: An example of shape modification with colors assigned to the control points and control polygon edges, where W, attached to the color bar, denotes the value of the weights of the control points.

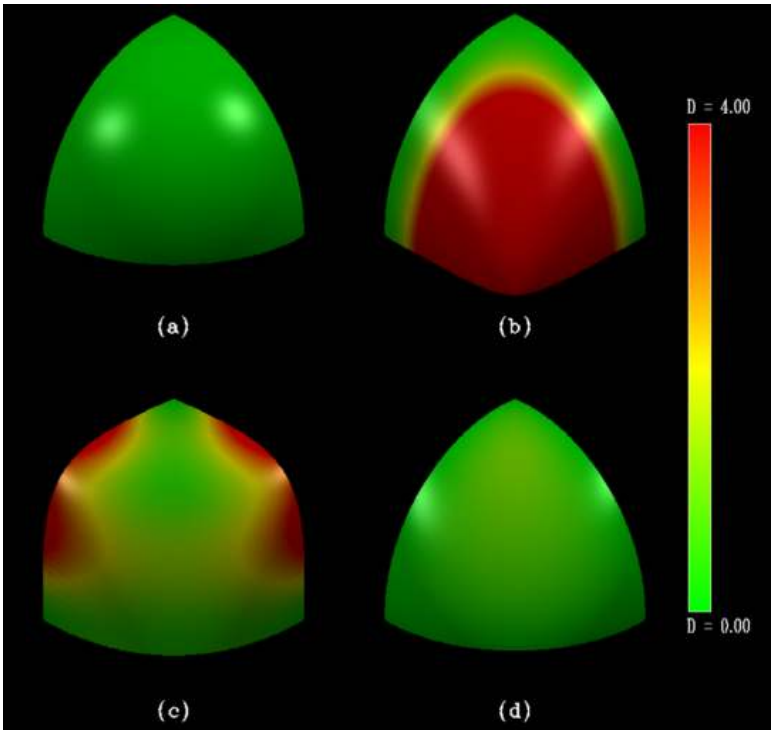

Figure 18: Deviations with colors for the shapes shown in Figure 17, where D, attached to the color bar, denotes the deviation defined by Equation (26). Clearly, (d) has minimum deviation among the three ((b),(c), and (d)).

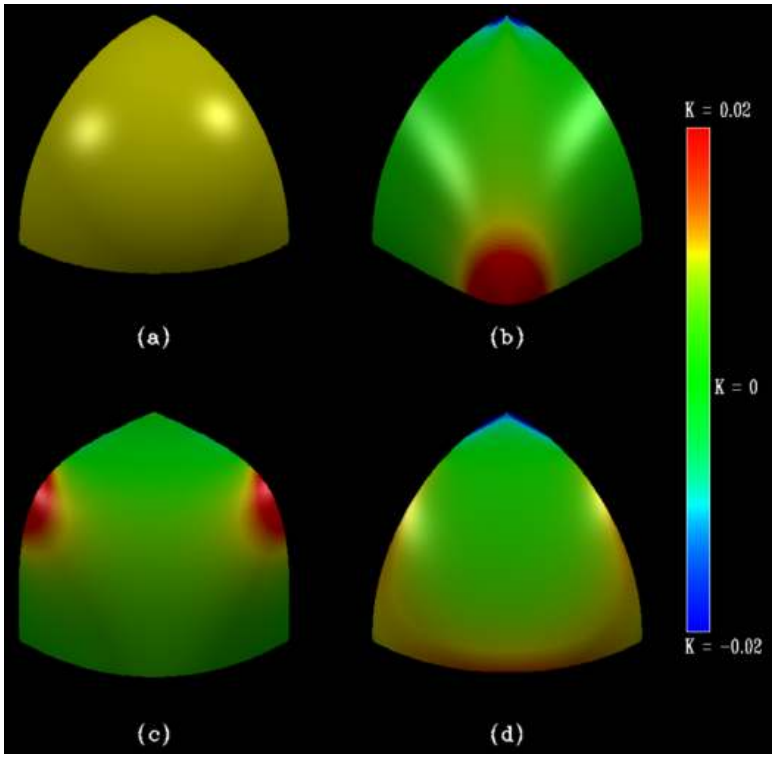

Figure 19: Gaussian curvatures with colors for the shapes shown in Figure 17.

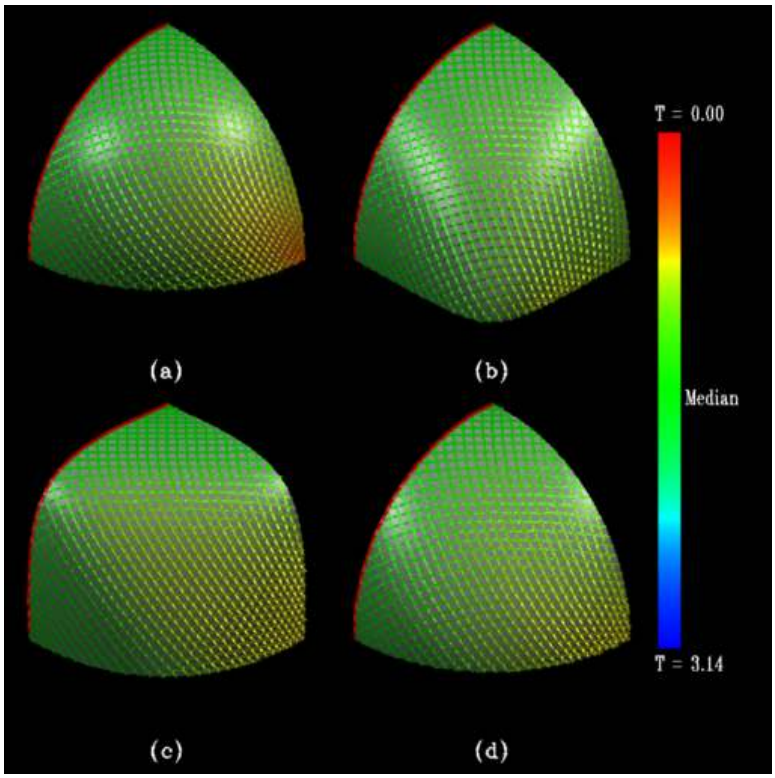

Figure 20: 3D fitting results with colors for the shapes shown in Figure 17.

to “darting” the excessive portion. For the breaking and bridging cases, it corresponds to “cutting” the cloth and “patching” the necessary portion. In the final approach the actual underlying surface is modified using constrained optimization in order to remove areas of high cloth deformation. If Equation (28) is not easily solved, a more complex approach involving the perturbation of control points and weights may be applied [3].

Finally, the Tchebychev net cloth model defined in Equation (2) can be extended by allowing extensions of weft and warp threads as follows:

$$\left.\begin{array}{l} |\mathbf{r}_x| = E_x \\ |\mathbf{r}_y| = E_y \end{array}\right\},$$

where E_x and E_y denote extension ratios of a weft thread and a warp thread, respectively. Similarly, the intersection problem described in Section 4 can be extended by dynamically changing the radii d^{weft} and d^{warp} at each crossing in Equation (16).

Acknowledgements

This project was partially supported by the Industrial Associates Program of the Rensselaer Design Research Center and the Overseas Scholarship Program of IBM Japan Ltd. Any opinions, findings, and conclusions expressed in this publication are those of the authors and do not necessarily reflect the views of any of the sponsors.

References

[1] Aono, M. (1990), A Wrinkle Propagation Model for Cloth, *Proc. CG International*, T.S. Chua and T.L.Kunii eds, Springer-Verlag, Tokyo, pp. 95-115.

[2] Aono, M., Breen, D.E., and Wozny, M.J. (1993), A Computer-aided Broadcloth Composite Layout Design System, 223-250, in: Wilson, P.R., Wozny, M.J., and Pratt, M.J., eds., *Geometric Modeling for Product Realization*, North-Holland.

[3] Aono, M. (1994), Computer-Aided Geometric Design for Forming Woven Cloth Composites, Ph.D. thesis, Department of Computer Science, Rensselaer Polytechnic Institute, Troy, NY.

[4] Aono, M., Breen, D.E., and Wozny, M.J. (1994), Fitting a Woven Cloth Model to a Curved Surface: Mapping Algorithms, *Computer Aided Design*, Vol. 26, No. 4, pp. 278-292.

[5] Aono, M., Denti, P., Breen, D.E., and Wozny, M.J. (1996), Fitting a Woven Cloth Model to a Curved Surface: Dart Insertion, *IEEE Computer Graphics and Applications*, Vol. 16, No. 5, pp. 60-70.

[6] Barnhill, R.E., Farin, G., Fayard, L., and Hagen, H. (1988), Twists, Curvatures, and Surface Interrogation, *Computer Aided Design*, Vol. 20, No. 6, pp. 341-346.

[7] Breen, D.E., House, D.H., and Wozny, M.J. (1994), Predicting the Drape of Woven Cloth Using Interacting Particles, *SIGGRAPH '94 Conference Proceedings*, Orlando, FL, July 1994, pp. 365-372.

[8] Dhande, S.G., Rao, P.V.M., and Moore, C.L. (1993), Geometric Modeling of Draped Fabric Surfaces, in *Graphics, Design and Visualization*, Mudur, S.P. and Pattanaik, S.N. eds, Jaico Publishing House, Bombay, pp. 173-180.

[9] DoCarmo, M. P. (1976), *Differential Geometry of Curves and Surfaces*, Prentice-Hall, Inc., Englewood Cliffs, NJ.

[10] Dowling, N. E. (1993), *Mechanical Behavior of Materials*, Prentice-Hall, Inc., Englewood Cliffs, NJ.

[11] Fan, J., Q. Wang, S.-F. Chen, M.M.F. Yuen, and C.C. Chan (1998), A Spring-Mass Model-Based Approach for Warping Cloth Patterns on 3D Objects, *Journal of Visualization and Computer Animation*, Vol. 9, pp. 215-227.

[12] Farin, G. (1992), *Curves and Surfaces for Computer Aided Geometric Design*, Third Edition, Academic Press Inc., San Diego, CA.

[13] Gregory, J. and Lin, C. (1992), *Constrained Optimization in the Calculus of Variations and Optimal Control Theory*, Van Nostrand Reinhold, New York, NY.

[14] Hazzidakis, J.N. (1880), Ueber einige Eigenschaften der Flächen mit constantem Krümmungsmass, *J. für die Reine und Angewandte Mathematik*, Vol. 88, pp. 68-73.

[15] Heisey, F.L. and Haller, K.D., "Fitting Woven Fabric to Surfaces in Three Dimensions," *Journal of the Textile Institute*, Vol. 79, No. 2, pp. 250-263 (1988)

[16] Hoskin, B.C. and Baker, A.A. (1986), *Composite Materials for Aircraft Structures*, AIAA Inc., New York, NY.

[17] Mack, C. and Taylor, H. M. (1956), The Fitting of Woven Cloth to Surfaces, *Journal of the Textile Institute*, Vol. 47, T477-488.

[18] Material Science Corporation (1986), Woven Fabric Reinforced Composites for Automotive Applications, Technical Report MSC TFR 1605/8102.

[19] McCartney, J., B.K. Hinds, and B.L. Seow (1999), The Flattening of Triangulated Surfaces Incorporating Darts and Gussets, *Computer Aided Design*, Vol. 31, pp. 249-260.

[20] Ng, H.N., and Grimsdale, R.L. (1996), Computer Graphics Techniques for Modeling Cloth, *IEEE Computer Graphics and Applications*, Vol. 16, No. 5, pp. 28-41.

[21] Pipkin, A. C. (1984), Equilibrium of Tchebychev Nets, *Arch. Rational Mech. Anal.*, Vol. 95, pp. 93-115.

[22] Potter, K. D. (1979), The Influence of Accurate Stretch Data for Reinforcements on the Production of Complex Structural Mouldings, *Composites*, pp. 161-173.

[23] B.G. Prakash, T. G. Simha, D. D. Sundararaju, D. D. Ravindranath, and K. G. Shatry, "AUTOLAY - An Interactive Graphics System for the Design of Aircraft Composite Components" in *Graphics, Design and Visualization* ed. by S. P. Mudur and S. S. Pattanaik, Jaico Publishing House, Bombay, India pp 189-197 (1993)

[24] Rivlin, R. S. (1964), Networks of Inextensible Cords, in *Nonlinear Problems of Engineering*, Ames, W.F. ed., Academic Press, pp. 51-64.

[25] Robertson, R.E., Hsiue, E.S., Sickafus, E.N., and Yeh, G.S.Y. (1981), Fiber Arrangements During the Modeling of Continuous Fiber Composites - I. Flat Cloth to a Hemisphere, *Polymer Composites*, Vol. 2, No. 3, pp. 126-131.

[26] D. F. Rogers, *Procedural Elements for Computer Graphics*. McGraw-Hill, Inc., New York, NY, 1998.

[27] Rudomin, I. J. (1990), Simulating Cloth Using a Mixed Geometric-Physical Method, Ph.D. thesis, Department of Computer and Information Science, the University of Pennsylvania, Philadelphia, PA.

[28] Samelson, S.L. (1989), Tchebychev Net on Two-Dimensional Riemannian Manifolds, Ph.D. thesis, Department of Mathematics, Carnegie Mellon University, Pittsburgh, PA.

[29] Samelson, S.L. (1991), Global Tchebychev Nets on Complete Two-Dimensional Riemannian Surfaces, *Arch. Rational Mech. Anal.* 114, 237-254.

[30] Stoker, J.J. (1969), *Differential Geometry*, John Wiley & Sons, Inc., New York, NY.

[31] Struik, D. J. (1961), *Lectures on Classical Differential Geometry*, Second Edition, Addison Wesley, Reading, MA.

[32] Tchebychev, P. L. (1878), Sur la coupe des vêtements, Assoc. Franç. pour l'Avancement des Sci., Congrès de Paris, 154-155, also available as "The Cutting out of Clothes," *Uspekhi matematicheskikh nauk*, Vol. 1, No. 2, pp. 38-42 (1946).

[33] Terzopoulos, D. and Fleischer, K. (1988), Deformable Models, *Visual Computer*, Vol. 4, pp. 306-331.

[34] Timoshenko, S.P. and Goodier, J.N. (1982), *Theory of Elasticity*, Third Edition, Mc-Graw-Hill, Inc.

[35] Van West, B.P., Pipes, R.B., and Keefe, M. (1990), A Simulation of the Draping of Bidirectional Fabrics over Arbitrary Surfaces, *Journal of the Textile Institute*, Vol. 81, pp. 448-460.

[36] Wang, W-B. (1986), Stress and Strain Analysis of Fibre-Reinforced Sheets with Bending Stiffness, Ph.D. thesis, Department of Applied Mathematics, Brown University, Providence, RI.

[37] Weil, J. (1986), The Synthesis of Cloth Objects, *Computer Graphics*, Vol. 20, No. 4, pp. 359-376.